NUMERICAL STUDY ON A THERMOACOUSTIC REFRIGERATOR WITH CONTINUOUS AND STAGGERED ARRANGEMENTS

by

Liu LIU and Yingwen LIU*

Key Laboratory of Thermo-Fluid Science and Engineering of MOE,
School of Energy and Power Engineering, Xi'an Jiaotong University, Xi'an, Shaanxi, China

Original scientific paper
https://doi.org/10.2298/TSC210901025L

Thermoacoustic devices require heat exchangers with oscillating flow, but there is currently no viable design approach for them. A heat exchanger with a staggered structure can efficiently improve the velocity disturbance and promote heat transfer in steady flow. The flow and heat transfer characteristics of a standing-wave thermoacoustic refrigerator and an ambient heat exchanger with staggered parallel plates under the oscillating flow condition are investigated in this study, primarily focusing on the geometric influences and differences between staggered and non-staggered (continuous) arrangements. The CFD simulation is a mainstream tool for the numerical simulation of complex thermoacoustic phenomena. The flow field around the stack and heat exchanger plate is simulated by introducing the dynamic mesh boundary conditions. Through numerical simulation, the flow field characteristics of non-linear vortices generation around the heat exchanger are presented. By changing the staggered column number in the ambient heat exchanger, it is observed that the larger the column number of staggered parallel plates, the more significant the refrigeration effect through the thermoacoustic effect.

Key words: *thermoacoustic, refrigerator, ambient heat exchanger, staggered, column number*

Introduction

A thermoacoustic refrigerator (TAR) is a device with no moving parts that transfers heat from a low temperature reservoir to a high temperature reservoir by utilizing acoustic power [1]. The acoustic driver, resonator, heat exchangers, and stack are the major components of standing-wave TAR. The acoustic driver is attached to the resonator filled with working gas. The stack and two heat exchangers consisting of many parallel plates are installed in the resonator.

The loss coefficient induced by the abrupt change in the cross-section of TAR, as well as non-linear phenomena such as vortices shedding and thermoacoustic streaming, are not taken into account in the standard thermoacoustic first-order linear model [2]. As a result, CFD simulation research is regarded as a necessary step in the analysis of non-linear systems. The first numerical simulation of the oscillating flow in a thermoacoustic system was studied by Cao *et al.* [3]. Worlikar *et al.* [4] used a low Mach number model to simulate the oscillating flow near 2-D parallel plates, followed by Besnoin and Kino [5]. Marx and Blanc-Benon [6]

* Corresponding author, e-mail: ywliu@xjtu.edu.cn

ran a numerical simulation of the stack's temperature differential at different Mach numbers. Jaworski and Piccolo [7] and Ilori *et al.* [8] studied whether different stack edge designs can help to lessen the flow complexity produced by the thermoacoustic system's geometric discontinuity. Therefore, numerical simulation is required to comprehend the thermoacoustic complex system's non-linear behavior, which supports the current experimental study.

The oscillating flow system involves various research fields (electricity [9], magnetism [10, 11], acoustics [12], thermodynamics [13]) and many researchers have conducted qualitative and quantitative studies on its heat transfer and flow mechanism. Kargarsharifabad *et al.* [14] and Asadikia *et al*. [15] provided experimental and numerical analyses of natural-convection heat transfer of the nanofluid in a cubic enclosure under the effects of both the time-unvarying and oscillating magnetic fields. Nsofor *et al.* [16] investigated the oscillating flow and heat transfer in the heat exchanger of a TAR system and obtained a new heat transfer correlation. Based on their research, Elaziz *et al.* [17] suggested an improved adaptive neuro-fuzzy inference system for predicting the oscillation heat transfer coefficient in the thermoacoustic heat exchangers. In a Stirling engine and pulse tube, Liu *et al.* [18] analyzed the influence of different pipe sections on the oscillating flow of the tubular heater and cooler. Wu *et al.* [19] quantified convective heat transfer and summarized the heat transfer characteristics of a staggered tube bundle heat exchanger in oscillating flow. The oscillating flow of the working medium is an important feature of a regenerative refrigerator/engine, and the heat transfer performance of heat exchangers operating in the oscillating field is one of the most pivotal aspects determining the efficiency of a regenerative refrigerator/engine.

To enhance convective heat transfer, many configurations have been modified to offset or staggered plates or fins, which are commonly employed in compact heat exchangers. The wake behind the plates or fins can interrupt the flow and cause it to become unstable, and the sinusoidal flow may be produced by the existence of discrete vortices [20]. The staggered fins or plates destroy the flow and temperature boundary-layer at the cross-sections and strengthen the heat dissipation, but the disadvantage is that the flow resistance increases. Suzuki *et al.* [21] employed numerical simulation to investigate the transient flow field and temperature of continuous plates and analyzed a series of spin pair heat transfer enhancements caused by the instability of oscillating flow between plates. Ali *et al*. [22, 23] used the edge effect caused by staggered plates to investigate the heat transfer mechanism in a solar air collector under steady laminar flow. The staggered heat exchanger can increase the disturbance in a steady flow, while the transition flow provides strong heat mixing without raising the friction coefficient, thus promoting heat transmission. Is it possible for the heat transfer of a parallel-plate heat exchanger in a standing-wave thermoacoustic system to be enhanced by the staggered design of the parallel-plate heat exchanger in oscillating flow? A staggered heat transmission structure was designed to optimize thermoacoustic oscillation and improve the refrigeration effect.

The heat transfer properties and flow field of the working fluid can be affected by a sudden change in the cross-section of the flow channel due to the presence of the stack and heat exchangers. In this study, CFD modelling is utilized to simulate a portion of the flow region of a standing-wave TAR using the dynamic mesh boundary condition. The ambient heat exchanger was used as the research object to investigate the effects of staggered plate structure and traditional continuous parallel-plate structure on the oscillating flow field and heat transfer properties of the thermoacoustic system. The heat transfer parallel plates were divided into two and three staggered columns, respectively, and the influence of staggered column number on refrigeration effect and non-linear flow structure was studied.

Materials and models

Device description

The standing-wave thermoacoustic refrigerator is half-wavelength ($\lambda/2$) long, as shown in fig. 1. The 2-D model inspired by El-Rahman and Abdel-Rahman [24] is used in this study to save computing costs associated with 3-D simulation. Figure 2 indicates the computational domains of the flow simulation with continuous and staggered parallel-plate arrangements of the ambient heat exchanger. The heat exchangers and stack are arranged in a regular pattern, reducing the entire domain to a narrow area with a height of H = 0.0008 m, which is referred to as the computational domain. Case 1 represents the baseline structure with the traditional continuous parallel-plate arrangement. The parallel plates in the ambient heat exchanger are separated into two columns and three columns in Cases 2 and 3, respectively. The staggered spacing between plates is the same in Cases 2 and 3, and the length of each plate is identical. The helium is the working gas, which is at a mean pressure of p_m = 1 MPa. The main parameters which are needed in the numerical computation are listed in tab. 1.

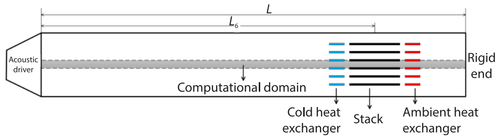

Figure 1. Schematic of the standing-wave thermoacoustic refrigerator

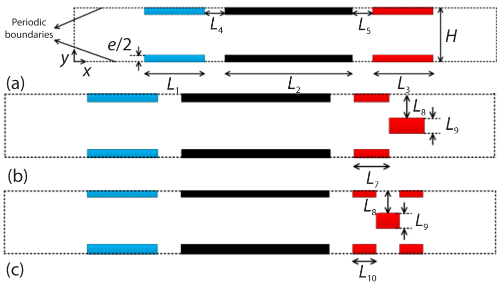

Figure 2. Computational domain of the flow simulation; (a) baseline model, Case 1, (b) two columns, Case 2, and (c) three columns, Case 3

Table 1. Parameters for the simulation

Structure parameters	L = 0.868 m	$L_1 = L_3$ = 0.009 m
	L_2 = 0.07 m	L_6 = 0.7577 m
	$L_4 = L_5 = L_9 = e$ = 0.0002 m	$L_8 = L_{10}$ = 0.0003 m
	L_7 = 0.00045 m	H = 0.0008 m
Physical properties	$\mu_f = 1.996 \cdot 10^{-05}$ Ns/m^2	$c_{p,f}$ = 5192.3 J/kgK
	k_f = 0.15665 W/mK	k_s = 16.27 W/mK
	$c_{p,s}$ = 502.48 J/kgK	a = 1023.4 m/s
	ρ_s = 8030 kg/m^3	ρ_f = 1.5974 kg/m^3
Operational conditions	p_m = 1 MPa	$T_h = T_m$ = 300 K

Governing equations

The commercial CFD software, FLUENT 14.0, is used for all the low Mach numerical simulation calculations. The governing equations are applied:

$$\frac{\partial \rho}{\partial t} + \nabla(\rho \mathbf{u}) = 0 \tag{1}$$

$$\rho \frac{\partial \mathbf{u}}{\partial t} + \nabla\left[\mathbf{u}(\rho \mathbf{u})\right] = -\nabla p + \mu \nabla^2 \mathbf{u} + \frac{\mu \nabla(\nabla \mathbf{u})}{3} \tag{2}$$

$$\rho c_p \frac{\partial T}{\partial t} + \rho c_p \mathbf{u} \nabla T = \frac{\partial p}{\partial t} + k_f \nabla^2 T + p \nabla \mathbf{u} + 2\mu \Phi \tag{3}$$

where T, p, $\mathbf{u}$, and ρ are the temperature, pressure, velocity vector, and density of the working gas, respectively. Besides, μ, k_f, t, and c_p are the refer to dynamic viscosity, fluid thermal conductivity, time, specific heat capacity, respectively, and Φ is the viscous dissipation function. At the solid-fluid interfaces, thermally coupled boundary conditions are imposed to simulate the thermal interactions between the surrounding gas particles and the solid walls through the conjugate heat transfer algorithm.

Boundary conditions and numerical resolutions

The computations are performed with a transient and double-precision solver. Since the fluid-flow in a thermoacoustic system can be regarded as a compressible low Mach number flow, a pressure-based solver is used. The numerical calculation is based on the laminar model. For pressure-velocity coupling, the SIMPLE scheme and the finite volume method are used. In addition, the discretization approach for second-order upwind space convective terms is used. The initial temperature of the thermoacoustic system is equal to that of the ambient heat exchanger and constant at 300 K. The heat exchangers and stack are made of copper and steel, respectively. More importantly, the dynamic mesh boundary condition is used to replace the role of the acoustic driver. The mesh deformation caused by dynamic mesh makes the thermoacoustic system form the oscillating flow. The dynamic velocity at the oscillating boundary, u_w:

$$u_w = u_a \sin(kx)\cos(2\pi f t), \ \ u_a = \frac{p_a}{\rho_m a} \tag{4}$$

where u_a, p_a, ρ_m, and a represent the velocity amplitude, pressure amplitude, mean density and the sound speed, respectively. The calculated resonance frequency f of the TAR system is 590 Hz (cycle time $\tau \approx 0.001695$ seconds). While k and x refer to the wavenumber and the axial position of the oscillating boundary.

Validation of independence and model

Grid size and time sensitivity analysis

Here, Case 1 is used for grid-independent testing. The structural grids are adopted and generated by the software GAMBIT. The grids near the parallel plates are denser. Figure 3(a) indicates heat transfer coefficients of the ambient heat exchanger among the three grid levels (coarse grid with 27554 cells, medium grid with 59684 cells, and fine grid with 98486 cells). The maximum difference between the three grid levels is only 1%. Therefore, the medium grid

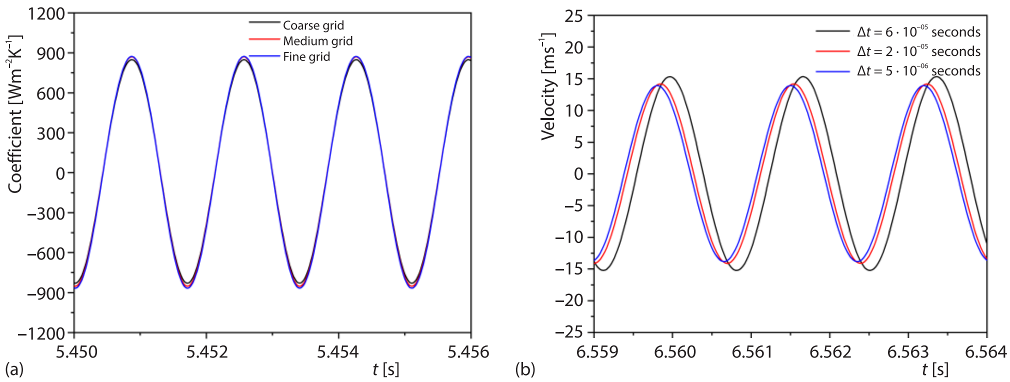

Figure 3. Grid and time independence study; (a) grid independence and (b) time independence (*for color image see journal web site*)

is enough to generate the independent result and adopted in the following numerical calculation. Otherwise, the time step is also significant in the unsteady numerical simulation. Three levels of the time step ($6 \cdot 10^{-05}$ seconds, $2 \cdot 10^{-05}$ seconds, and $5 \cdot 10^{-06}$ seconds) are selected to perform the simulation in fig. 3(b). The axial velocities at a monitoring point (x = 0.5 m, y = 0.0004 m) in different cases are compared. The onset time step which triggers the oscillation is $6 \cdot 10^{-05}$ seconds. Compared with the other two cases, the relatively large time step of $6 \cdot 10^{-05}$ seconds has some differences in the amplitude and phase of velocity fluctuation. The simulation results with the time step of the $2 \cdot 10^{-05}$ seconds and $5 \cdot 10^{-06}$ seconds are similar, so the time step of $2 \cdot 10^{-05}$ seconds is used for CFD simulation.

Model validation

In fig. 4(a), the time-averaged energy flux along the stack is compared with the results of Mergan *et al*. [25]. The time-averaged energy flux at both ends of the stack forms a sharp peak. In contrast, the time-average energy near the centre of the stack does not change much, which demonstrates that the heat exchange between the stack and gas is majorly at both ends of the stack. The peak breadth widens gradually with the computing time. The system is stable and the peak breadth remains unchanged when the computation time reaches 6 seconds. The analysis of fig. 4(a) depicts that the results achieved in this study are consistent with those of Mergan *et al*. [25]. Otherwise, According to [26], the relevant CFD numerical model was reestablished and compared with the experimental and theoretical data in this reference. The results are shown in fig. 4(b). At a lower frequency of 14.2 Hz, experimental values are slightly higher than the values predicted by the CFD and theoretical formulas. With the increase of drive ratio, the gaps among CFD, experimental and theoretical results increase. Within the limits of experimental work and theoretical predictions, the trend and value of CFD model calculation are adequate to verify its trustworthiness.

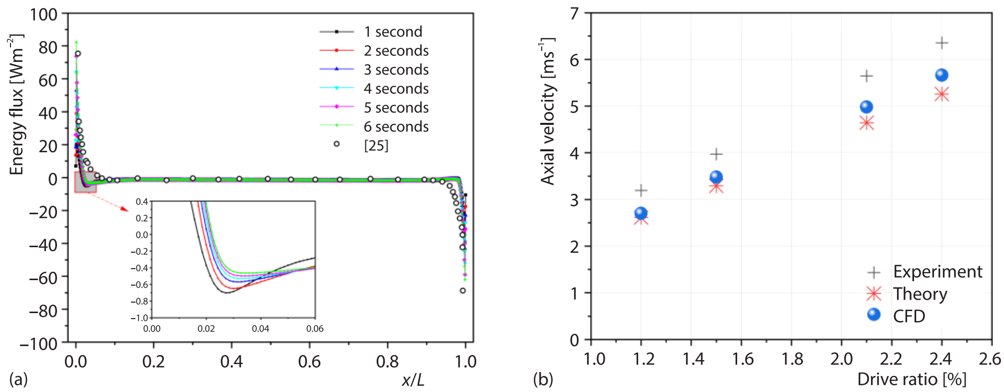

Figure 4. Validation of the CFD model; (a) energy flux density over the stack and (b) compared with the [26] (*for color image see journal web site*)

Results and discussion of RSM

Temperature analysis on the stack

Figure 5(a) shows the change of temperature at the ambient end of the stack with computation time. The temperature oscillates periodically when the thermoacoustic oscillation achieves saturation. With the increase of the number staggered column number, the frequency decreases from 587.3 Hz (Case 1, $\tau \approx 0.001703$ seconds) to 589.0 Hz (Case 2, $\tau \approx 0.001698$ seconds), and finally to 590.3 Hz (Case 3, $\tau \approx 0.001694$ seconds). The frequency of the staggered structure is higher than that of the continuous structure, despite the clear change in ambient heat exchanger structure having minimal effect on the system frequency. This is because the heat transfer between the gas and the stack is expedited, the heat transfer lag is decreased, and the temperature in the stack reaches a stable gradient distribution sooner. This demonstrates how the staggered structure can increase the resonant frequency and bring it closer to the calculated resonant frequency. At the middle of the cold and ambient heat exchangers, monitoring surfaces are set to obtain the temperature difference between the two ends of the stack. Figure 5(b) depicts the variation of the stack temperature difference obtained in different cases with the computing time. The final stable temperature differences for Cases 1-3 are 3.56 K, 3.87 K, and 4.05 K, respectively. The staggered structure has apparent advantages over the traditional continuous structure in that it produces a larger temperature differential, and the growth rate of temperature difference decreases as the number of staggered columns increases.

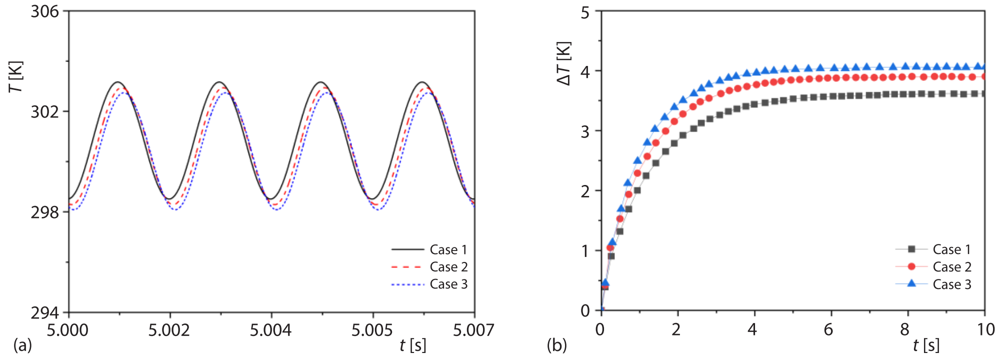

Figure 5. Temperature distributions under different cases; (a) stable oscillating state (b) temperature difference

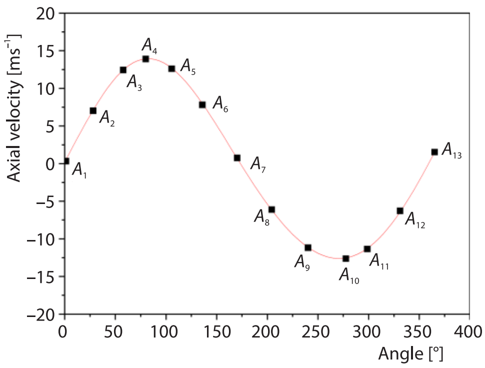

Figure 6. The changes of axial velocity with time over one flow cycle

Analysis of streamlines

Different from the steady flow, the magnitude and direction of velocity vary with time under the oscillating flow condition. To monitor velocity oscillation, an iso-surface is monitored at the centre of the ambient heat exchanger (x = 0.7975 m, y = 0.0004 m). Figure 6 shows the changes of axial velocity with time over one flow cycle. Considering the instantaneity and periodicity of the oscillating flow, the velocity oscillation in one cycle is divided into 12 subphases at an interval of 30°. Phases A_1-A_7 (representing 0°, 30°, 60°, 90°, 120°, 150°, and 180°, respectively) are used to analyze the change in the vortices flow.

The instantaneous streamline distribution of oscillating flow in different heat exchanger structures throughout half a cycle, as presented in fig. 7. Streamlines are a group of curves that are always tangent to the flow velocity vector. These depict the path that a massless fluid element will travel at any given time. The velocity magnitude aligned with the channel center is larger because of transverse area contraction when entering the channel. The gap between

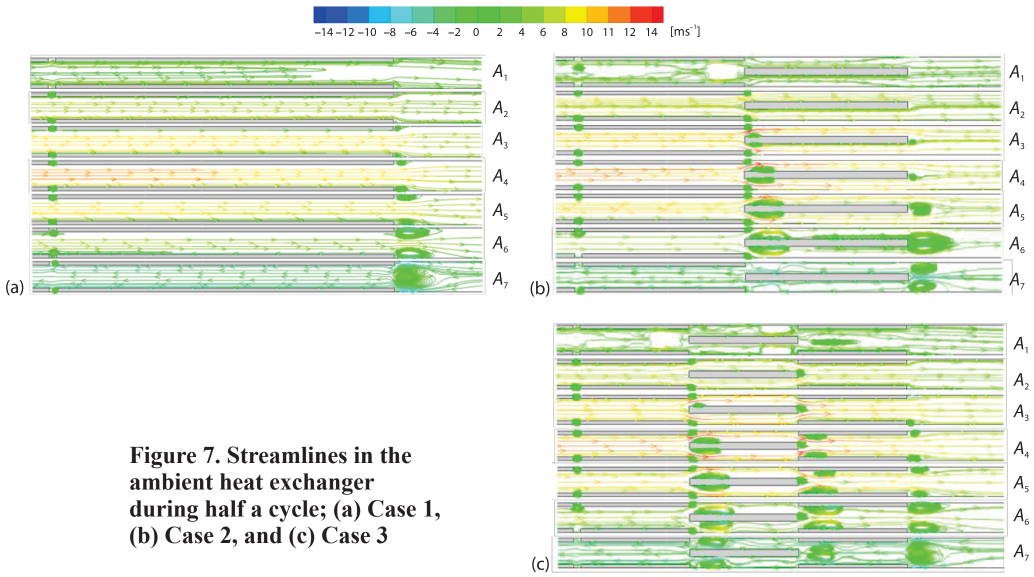

Figure 7. Streamlines in the ambient heat exchanger during half a cycle; (a) Case 1, (b) Case 2, and (c) Case 3

the left end of the ambient heat exchanger and the stack is small, and there is a streamline passing through this area when the flow velocity is small. With the increase of flow velocity, smaller vortices are gradually formed in this spacing. Moreover, the right end of the ambient heat exchanger has enough flow area. A pair of reverse vortices emerge near those ends with the increase of flow velocity, and their regions gradually expand. The streamline of the fluid-flow through the plate section shrinks first and then expands. The vortices are accompanied by the streamlined rotation at the front and rear of the parallel plates, which is caused by variable cross-sections and turbulent perturbations. The acoustic response in flow channels can be triggered by a temperature gradient. However, owing to the influence mechanism of fluid viscosity, the flow direction of the fluid near the plate wall remains unchanged in Case 1.

In Cases 2 and 3, the staggered arrangement and shorter plate length increase gas velocity near the plate wall and increase gas disturbance. The rotational range of streamlines steadily grows as the velocity ($A_2 \rightarrow A_3$) rises, implying that more streamlines travel between the staggered plates and the vorticity increases at the same time. When the velocity decreases ($A_5 \rightarrow A_6$), the rotational range of streamlines increases gradually, more streamlines change direction on both sides of the plate, and the vorticity increases accordingly. The phase with negative velocity can be regarded as an inverse process because of the periodicity of oscillating flow. When compared to other heat exchanger configurations, the boundary-layer breaks up before it accumulates on the plate because of the greater staggered column and shorter length in the flow direction. Flow vortices only form on the wall and corner of the abruptly changing cross-section, and the turbulence of the fluid is increased by disturbing the wake. The production and transformation of vortices correlate to the periodic fluctuation and rotation of streamlines.

Vorticity fields under different cases

To further separate the impacts of geometry structures and boundary-layer reconstruction mechanism caused by the plate arrangement, we choose six representative phase points: A_1, A_3, A_5, A_7, A_9, and A_{11} (representing 0°, 60°, 120°, 180°, 240°, and 300°, respectively). A vortex is an area in a fluid where the flow spins around an axis line that might be straight or curved in fluid dynamics. The fluid-flow velocity in most vortices is greatest near the axis and decreases in inverse proportion to the distance from the axis. Figure 8 compares the vorticity fields under different cases. A pair of counter-rotating vortices are formed attached to the end of the plates. Periodic vortex shedding phenomena are observed on various structures, and they induce periodic transverse forces on them, and they are ex-cited in the transverse direction. In Case 1, gas particles accelerate from left to right at A_3 moment, and a pair of vortices can be seen at plate ends but still adhere to them. When the velocity decreases gradually from the maximum value, the vortices are wholly separated from the plate ends. When the fluid reverses, vortices are gradually generated at the other ends of parallel plates. The vortices only change along the wall of the suddenly changed cross-section when the velocity changes. There is no vortex in most portions of the flow field because the streamline travels right through the sudden-changed cross-sections. The vortex breakup could be induced as a result of the pressure gradient and general instability due to high vorticity concentrations when the flow accelerates.

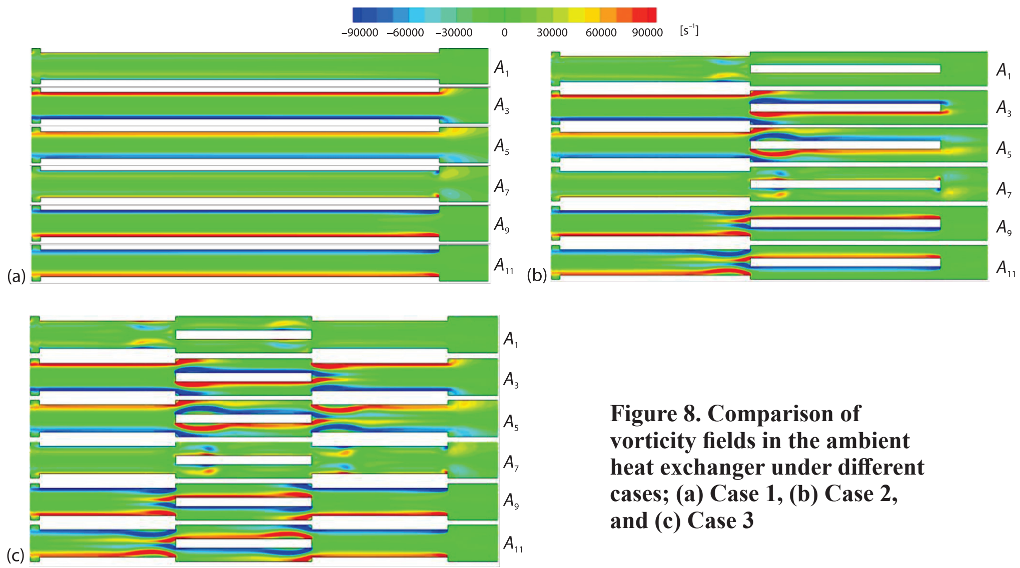

Figure 8. Comparison of vorticity fields in the ambient heat exchanger under different cases; (a) Case 1, (b) Case 2, and (c) Case 3

The vortex pairs in Case 2 are oblate and lengthy, indicating that the vortex has a wide range of impact on the fluid environment around it. This is since the velocity at the abrupt cross-section is substantially greater than the velocity inside the resonator. Such a large velocity difference necessitates a long buffer zone before it is entirely mixed with the velocity difference inside the resonator. The flow develops upstream as the velocity changes in the reverse direction, the right vorticity intensity gradually declines, and the left vorticity intensity gradually increases. The flow inside the plate changes noticeably as the staggered plates increase the fluid disturbance, and the dispersion of the vortices becomes dense and visible. The distribution of vorticity increases noticeably in Case 3. In general, during the oscillation period, the formation, growth, shedding, and dissipation processes are still accomplished. When compared to a continuous plate structure, the staggered arrangement can greatly increase fluid disturbance. The velocity difference at the front and rear of the sudden-changed cross-section gradually increases as the stagger column number increases, leading to an increase in vorticity intensity and the range of vortices influence, from concentrating near the wall of the sudden-changed cross-section gradually occupying the entire resonator.

Parameter distribution and performance

The distribution of velocity variation along the *x*-axis in a cycle time is analyzed to understand the changes of streamlines and vortices, as seen in fig. 9. The velocity variation of the ambient heat exchanger is also depicted in detail. The peak and valley values of velocity appear in different sizes within the influence range of vortices in the sudden-changed cross-sections, which determines the vorticity intensity. Even if the average velocity is still zero, the velocity fluctuation is symmetrical at different phases. The peak and valley values increase as the vorticity intensity increases. The velocity has a tiny peak and valley value in the staggered heat exchanger, which is related to the formation of vortices near the wall of the sudden-changed cross-section. The number of staggered plates in the ambient heat exchanger increases continuously from Cases 1-3, and the vorticity intensity increases as the number of sudden-changed cross-sections increases. Otherwise, the velocity fluctuation at the plate end is negligible due to the big enough flow area at the right end of the ambient heat exchanger. Consequently, the peak value and valley value of the time-average velocity steadily rise, which significantly increases the heat transfer of the ambient heat exchanger. As the number of staggered columns increases, the temperature of the ambient end decreases, aiding in the improvement of the refrigeration effect.

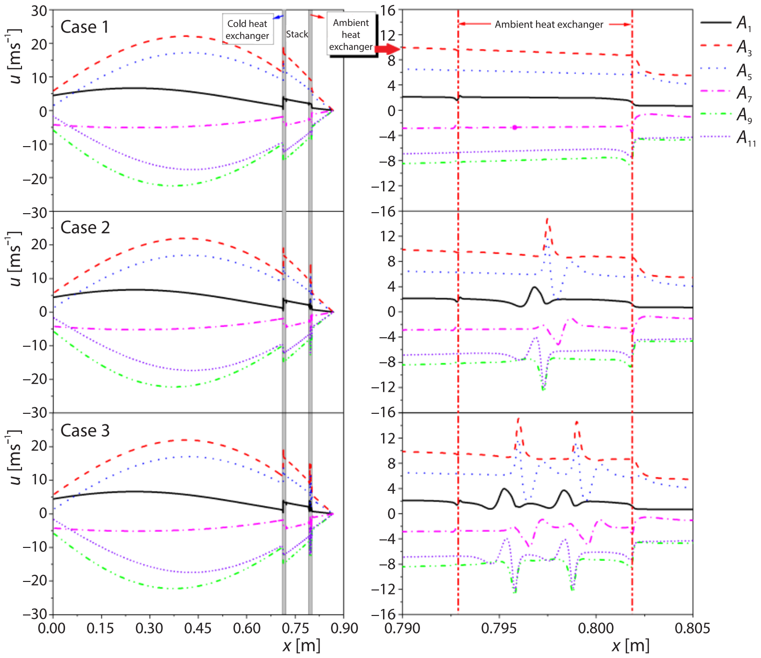

Figure 9. Velocity fluctuation along the *x*-axis within a period for different cases

The amplitudes of pressure drop and heat transfer coefficient of the ambient heat exchanger in different cases are illustrated in tab. 2. The streamline changes as the oscillating flow passes through the abrupt-changed cross-sections due to the sudden contraction and expansion of the flow area, resulting in vortices and pressure drop. The maximum heat transfer coefficient increases progressively as the number of staggered columns rises, but the rate of increase slows. Meanwhile, the amplitude of pressure drop diminishes and subsequently grows, with Case 1 having the biggest pressure drop. The coefficient of performance will be further reduced after considering the loss of heat conductivity and viscosity. Although the gas disturbance in the heat exchanger becomes more severe when the three-column staggered construction is increased, the heat transfer coefficient increases due to the pressure drop induced by friction loss caused by the viscous effect. It is an ideal method to enhance the heat transfer coefficient and reduce the pressure drop by adopting the ambient heat exchanger with staggered parallel plates.

Table 2. The thermal parameters in different cases

	Δp_a [bar]	h_a [Wm^{-2}K^{-1}]
Case 1	1023.8	298128.7
Case 2	1036.4	296872.5
Case 3	1043.1	296985.6

Conclusion

In this study, the standing-wave TAR with continuous and staggered ambient heat exchanger structures are simulated by using the dynamic mesh boundary condition. The CFD modelling revealed the refrigeration effect in the stack as well as non-linear vortices surrounding the heat exchanger plate. Compared with the traditional continuous structure, the surface discontinuity of the staggered structure prevents the thermal boundary-layer from growing continuously through periodic discontinuities. Furthermore, the refrigeration effect of the continuous structure is lower than that of the two staggered structures, indicating that the higher the number of staggered columns, the greater the temperature differential. Therefore, a well-designed staggered column number of the ambient heat exchanger can contribute to the improvement of the cooling impact of the thermoacoustic system. In the future, both the effects of the deviation distance between staggered plates in the ambient heat exchanger and the deviation distance between the heat exchanger and stack on the system performance will be studied.

Acknowledgment

This work was supported by the National Natural Science Foundation of China (No. 51976146).

Nomenclature

a – sound speed, [ms^{-1}]
e – plate thickness, [m]
f – frequency, [Hz]
H – height of the active cell, [m]
h – heat transfer coefficient, [Wm^{-2}K^{-1}]
L – length, [m]
n – normal, [–]
p – pressure, [Pa]
T – temperature, [K]
t – time, [s]
u – velocity in x-direction, [ms^{-1}]
$\mathbf{u}$ – velocity vector, [ms^{-1}]

Greek symbols

k – thermal conductivity, [Wm^{-1}K^{-1}]
λ – wavelength, [m]
μ – dynamic viscosity, [Nsm^{-2}]
ρ – density, [kgm^{-3}]
τ – cycle time, [second]

Subscripts

a – amplitude
f – fluid
m – mean
s – solid
w – wall

References

[1] Namdar, A., *et. al*, Numerical Investigation of Thermoacoustic Refrigerator at Weak and Large Amplitudes Considering Cooling Effect, *Cryogenics, 67* (2015), Jan., pp. 36-44
[2] El-Rahman, A. A., *et al.,* A 3-D Investigation of Thermoacoustic Fields in a Square Stack, *Int. J. Heat. Mass. Tran., 108* (2017), Part A, pp. 292-300

[3] Cao, N., *et al.*, Energy Flux Density in a Thermoacoustic Couple, *Journal Acoust. Soc. Am., 99* (1996), 6, pp. 3456-3464
[4] Worlikar, A. S., *et al.*, Numerical Simulation of a Thermoacoustic Refrigerator: II. Stratified Flow Around the Stack, *Journal Comput. Phys., 144* (1998), 2, pp. 299-324
[5] Besnoin, E., Knio, O. M., Numerical Study of Thermoacoustic Heat Exchangers in the Thin Plate Limit, *Numer. Heat. Transfer, Part A., 40* (2001), 5, pp. 445-471
[6] Marx, D., Blanc-Benon, P., Numerical Calculation of the Temperature Difference between the Extremities of a Thermoacoustic Stack Plate, *Cryogenics*, *45* (2005), 3, pp. 163-172
[7] Jaworski, A. J., Piccolo, A., Heat Transfer Processes in Parallel-Plate Heat Exchangers of Thermoacoustic Devices – Numerical and Experimental Approaches, *Appl. Therm. Eng*., *42* (2012), Sept., pp. 145-153
[8] Ilori, O. M., *et al*., Experimental and Numerical Investigations of Thermal Characteristics of Heat Exchangers in Oscillatory Flow, *Appl. Therm. Eng*., *144* (2018), Nov., pp. 910-925
[9] Chamkha, A. J., *et al*., Magnetohydrodynamic Mixed Convection and Entropy Analysis of Nanofluid in Gamma-Shaped Porous Cavity, *Journal Thermophys. Heat Trans*f., *34* (2020), 10, pp. 1-12
[10] Bahmani, A., Kargarsharifabad, H., Magnetohydrodynamic Free Convection of Non-Newtonian Power-Law Fluids over a Uniformly Heated Horizontal Plate, *Thermal Science*, *24* (2020), 2, pp. 1323-1334
[11] Bahmani, A., Kargarsharifabad, H., Laminar Natural-Convection of Power-Law Fluids over a Horizontal Heated Flat Plate, *Heat Transf. Asian Re*., *48* (2019), 3, pp. 1044-1066
[12] Manevitch, L. I., Vakakis, A. F., Non-Linear Oscillatory Acoustic Vacuum, *SIAM J. Appl. Math*., *74* (2014), 6, pp. 1742-1762
[13] Bouvier, P., *et al*., Experimental Study of Heat Transfer in Oscillating Flow, *Int. J. Heat. Mass. Tran*., *48* (2005), 12, pp. 2473-2482
[14] Kargarsharifabad, H., Experimental and Numerical Study of Natural-Convection of Cu-Water Nanofluid in a Cubic Enclosure under Constant and Alternating Magnetic Fields, *Int. Commun. Heat Mass Transf*., *119* (2020), 8, 104957
[15] Asadikia, A., *et al*., Characterization of Thermal and Electrical Properties of Hybrid Nanofluids Prepared with Multi-Walled Carbon Nanotubes and Fe_2O_3 Nanoparticles, *Int. Commun. Heat Mass Transf.*, *117* (2020), 104603
[16] Nsofor, E. C., *et al.*, Experimental Study on the Heat Transfer at the Heat Exchanger of the Thermoacoustic Refrigerating System, *Appl. Therm. Eng.*, *27* (2007), 14-15, pp. 2435-2442
[17] Elaziz, M. A., *et al.*, Improved Prediction of Oscillatory Heat Transfer Coefficient for a Thermoacoustic Heat Exchanger Using Modified Adaptive Neuro-Fuzzy Inference System, *Int. J. Refrig., 102* (2019), June, pp. 47-54
[18] Liu, B. Q., *et al.*, Theoretical Model of a Stirling/Pulse Tube Hybrid Refrigerator and Its Verification, *Appl. Therm. Eng., 189* (2021), 116587
[19] Wu, Z. J., *et al.*, Experimental Investigation on Heat Transfer Characteristics of Staggered Tube Bundle Heat Exchanger Immersed in Oscillating Flow, *Int. J. Heat. Mass. Tran., 148* (2020), Feb., pp. 119-125
[20] Erguvan, M., Macphee, D. W., Second Law Optimization of Heat Exchangers in Waste Heat Recovery, *Int. J. Energy. Res., 43* (2019), 11, pp. 5714-5734
[21] Suzuki, K., *et al.*, Mechanism of Heat Transfer Enhancement Due to Self-Sustained Oscillation for an in-Line Fin Array, *Int. J. Heat. Mass. Transfer., 37* (1994), l, pp. 83-96
[22] Ali, A. H. H., *et al.*, Investigation of Heat Transfer and Fluid-Flow in Transitional Regime Inside a Channel with Staggered Plates Heated by Radiation for PV/T System, *Energy, 59* (2013), 9, pp. 255-264
[23] Ali, A. H. H., Design Optimization of Staggered Plates' Channel Heated by Radiation Heat Flux Based on the Convective Heat Transfer and Fluid-Flow for Hybrid Photovoltaic/Thermal System, *Sustain. Energy, Techn., 19* (2017), 12, pp. 1-20
[24] El-Rahman, A. A., Abdel-Rahman, E., Computational Fluid Dynamics Simulation of a Thermoacoustic Refrigerator, *Journal Thermophys. Heat. Transf., 28* (2014), 1, pp. 78-86
[25] Mergen, S., *et al.*, Numerical Study on Effects of Computational Domain Length on Flow Field in Standing Wave Thermoacoustic Couple, *Cryogenics, 98* (2019), Mar., pp. 139-147
[26] Allafi, W. A., *et al.*, Fluid Dynamics of Oscillatory Flow Across Parallel-Plates in Standing-Wave Thermoacoustic System with Two Different Operation Frequencies. *Eng. Sci. Technol.*, *24* (2021), 1, pp. 41-49

Paper submitted: September 1, 2021
Paper revised: November 9, 2021
Paper accepted: December 2, 2021